Modeling Binding Kinetics at the Q_A Site in Bacterial Reaction Centers[†]

Jennifer Madeo and M. R. Gunner*

Physics Department J-419 City College of New York 138th Street and Convent Avenue, New York, New York 10031

Received March 24, 2005; Revised Manuscript Received June 18, 2005

ABSTRACT: Bacterial reaction centers (RCs) catalyze a series of electron-transfer reactions reducing a neutral quinone to a bound, anionic semiquinone. The dissociation constants and association rates of 13 tailless neutral and anionic benzo- and naphthoquinones for the Q_A site were measured and compared. The K_d values for these quinones range from 0.08 to 90 μM. For the eight neutral quinones, including duroquinone (DQ) and 2,3-dimethoxy-5-methyl-1,4-benzoquinone (UQ_0), the quinone concentration and solvent viscosity dependence of the association rate indicate a second-order rate-determining step. The association rate constants (k_{on}) range from 10^5 to 10^7 M^{-1} s^{-1}. Association and dissociation rate constants were determined at pH values above the hydroxyl pK_a for five hydroxyl naphthoquinones. These negatively charged compounds are competitive inhibitors for the Q_A site. While the neutral quinones reach equilibrium in milliseconds, anionic hydroxyl quinones with similar K_d values take minutes to bind or dissociate. These slow rates are independent of ionic strength, solvent viscosity, and quinone concentration, indicating a first-order rate-limiting step. The anionic semiquinone, formed by forward electron transfer at the Q_A site, also dissociates slowly. It is not possible to measure the association rate of the unstable semiquinone. However, as the protein creates kinetic barriers for binding and releasing anionic hydroxyl quinones without greatly increasing the affinity relative to neutral quinones, it is suggested that the Q_A site may do the same for anionic semiquinone. Thus, the slow semiquinone dissociation may not indicate significant thermodynamic stabilization of the reduced species in the Q_A site.

Photosynthetic reaction centers (RCs)[1] are integral membrane proteins that catalyze light-initiated electron-transfer reactions across the cell membrane. In the bacteria *Rhodobacter sphaeroides*, RCs have nine bound cofactors embedded in three polypeptide chains (L, M, and H). These cofactors are arranged in two symmetric branches spanning the membrane (*1*). The primary electron donor P, a bacteriochlorophyll dimer, absorbs a photon obtaining the energy to reduce the active branch bacteriopheophytin (H_A). The reduced $H_A^{·-}$ in turn reduces the primary quinone, Q_A, resulting in the $P^+Q_A^{·-}$ state, separating charge 25 Å across the cell membrane. $Q_A^{·-}$ reduces the secondary quinone, Q_B, yielding $P^+Q_B^{·-}$. In isolated RCs, charge recombination, reducing P^+, competes with forward electron transfer. This can occur from $Q_B^{·-}$, from $Q_A^{·-}$ when the Q_B-binding site is empty, or from $H_A^{·-}$ if the Q_A site is empty (*2, 3*).

In *Rb. sphaeroides* RCs, the quinone in the Q_A and Q_B sites are both ubiquinone-10 (UQ_{10}). The Q_A- and Q_B-binding sites have different affinities for the various UQ_{10} redox states, allowing them to play different functional roles. Thus, electron transfer from $Q_A^{·-}$ to Q_B is favorable despite their chemical identity (*4*). Q_A accepts only one electron, forming the semiquinone, while two cycles of electron transfer forms the doubly reduced quinol at the Q_B site (*5, 6*). The quinol dissociates rapidly allowing another free quinone to bind the Q_B site and restart the cycle (*7, 8*).

The redox midpoint potentials (E_m) for semiquinone formation are difficult to measure in water because quinones are reduced directly to the dihydroquinone, without formation of a stable semiquinone intermediate (*4, 9*). However, a variety of studies place the E_m values for UQs higher in the Q_A and Q_B sites relative to the aqueous solution (*4, 10−12*). A shift in E_m requires that the product semiquinone binds more tightly than the neutral reactant quinone (*4*). However, because semiquinones are not stable in solution, their affinity cannot be measured directly by titration. Previous studies measuring the semiquinone lifetime in the binding site have shown that the anionic semiquinone dissociates more slowly than the neutral quinone (*13, 14*). As long as k_{on} slows less than k_{off}, the semiquinone K_d would be tighter than the neutral, in agreement with the E_m being higher in the protein.

Hydroxyl quinones at pH values above their pK_a values are stable anionic inhibitors at the Q_A site whose association and dissociation rates can be directly measured. The work presented here measures the association rate constants for functional neutral and anionic hydroxyl quinones at the Q_A site of RCs from *Rb. sphaeroides*. The binding mechanism is determined, and the correlation of affinity with the dissociation rate is compared. Parallels between binding the anionic hydroxyl quinones and the semiquinone formed in the Q_A site by the electron-transfer reaction are explored.

MATERIALS AND METHODS

RC Isolation and Activity. Rb. sphaeroides polyhistidine-tagged RCs were isolated as described previously (*15*). The RCs were purified on Ni−NTA (nitrilotriacetic acid) resin. The Ni−NTA column was washed with 0.05% LDAO in 10 mM Tris buffer, and the RCs were eluted with 40 mM imidazole in 0.05% LDAO at pH 8. Q_A removal (*10, 16*) yielded RCs with less than 10% of the native ubiquinone left in the Q_A site and empty Q_B sites. The RC concentration was determined given $\epsilon_{802} = 0.288 \ \mu M^{-1} \ cm^{-1}$. A 10 μs xenon flash excited the ground-state RCs and formed the charge-separated state, $P^{\cdot+}Q_A^{\cdot-}$ ($RCQ^{\pm}$). A photomultiplier tube monitored the $P^{\cdot+}$ signal at 430 nm. The concentration of $RCQ^{\pm}$ was obtained from the initial amplitude change $\approx$100 μs after the flash obtained given $\epsilon_{430} = 8.69 \times 10^3$ ΔOD/M.

Determining Q_A-Binding Affinity. The amplitude of the ΔA_{430} is directly proportional to the RCQ concentration (eq 1)

$$RCQ = \left(\frac{\Delta A - \Delta A_{min}}{\Delta A_{max} - \Delta A_{min}}\right) RC_T \qquad (1)$$

where RC_T is the total RC concentration. ΔA_{min} is the flash-induced amplitude change found before quinone addition because of the 5−10% residual ubiquinone-10 left in the Q_A site. ΔA_{max} is the amplitude when all RCs have bound a functional quinone. The best fit for the dissociation constant (K_d) was determined from eq 2 using the dependence of ΔA_{430} on the total quinone concentration (Q_T) using the Levenberg−Marquardt fitting program in IGOR Pro (Wave-Metrics)

$$\Delta A(Q_T) = \left(\frac{\Delta A_{max} - \Delta A_{min}}{2RC_T}\right)[K_d + Q_T + RC_T - \sqrt{-4Q_T RC_T + (K_d + Q_T + RC_T)^2}] \qquad (2)$$

Eight neutral, active quinones [2-bromo-naphthoquinone (2-Br-NQ), 2,3-dimethyl-naphthoquinone (2,3-diMe-NQ), 2-methoxy-naphthoquinone (2-MeOx-NQ), 2-methyl-naphthoquinone (2-Me-NQ), tetramethyl-benzoquinone (duroquinone, DQ), 1,2-naphthoquinone (1,2-NQ), 1,4-naphthoquinone (1,4-NQ), and 2,3-dimethoxy-5-methyl-1,4-benzoquinone (UQ₀)] and five hydroxyl quinones [5-hydroxy-3-methyl-naphthoquinone (5-OH-3-Me-NQ), 5-hydroxy-naphthoquinone (5-OH-NQ), 2-hydroxy-3-isopropyl-naphthoquinone (2-OH-3-Iso-NQ), 2-hydroxy-3-methyl-naphthoquinone (2-OH-3-Me-NQ), and 2-hydroxy-naphthoquinone (2-OH-NQ)] purchased from Sigma were studied.

Hydroxyl quinones at pH values above their pK_a are anionic competitive inhibitors of the Q_A site. K_I values were determined by the ability of the inhibitors to displace the functional duroquinone (DQ) from the Q_A site, diminishing ΔA_{430}. The equilibrium amplitude of active RCs was determined as a function of the inhibitor concentration with 30 μM DQ ($K_d = 0.4 \ \mu M$), 1 μM RCs, 0.005% LDAO, and 10 mM buffer. Tris was used at pH 7.8, and Caps was used for measurements at pH 10.2. The K_I was obtained fitting eqs 3 and 4 with Mathematica 4.2. Here, RCQ is the concentration of duroquinone-bound RCs and RCI is the concentration of hydroxyl quinone-bound RCs

$$K_d = \frac{(RC_T - RCQ - RCI)(Q_T - RCQ)}{RCQ} \qquad (3)$$

$$K_I = \frac{(RC_T - RCQ - RCI)(I_T - RCI)}{RCI} \qquad (4)$$

Determining Hydroxyl Quinone pK_a Values in Solution. The pK_a values for the five hydroxyl quinones were determined using the difference absorbance spectra of the ionized species relative to the neutral measured between 450 and 530 nm. Succinic acid (pH 3−5), Mes (pH 5.5−6.5), Tris (pH 7.5−8.5), Ches (pH 9−10), and Caps (pH 10.5−11.5) were used as buffers. The data were fit to eq 5, where ΔA is the absorbance relative to that found at pH 3 and ΔA_{max} is the absorbance at pH 11 minus that at pH 3. The pK_a values and wavelengths monitored for each quinone are listed in Table 2

$$pH = pK_a + \log\left(\frac{QO^-}{QOH}\right) = pK_a + \log\left(\frac{\Delta A}{\Delta A_{max} - \Delta A}\right) \qquad (5)$$

Quinone Association Rate Constants. The change in $RCQ^{\pm}$ monitored by ΔA_{430} following a second flash was used to derive the second-order association rate constant (k_{on}) for the active, neutral quinones (see the caption of Figure 1 and the Supporting Information for a more complete description of the model). The sample has 0.9−1.1 μM RC, 10 mM Tris, and 0.005% LDAO at pH 8, and the Q_B site is empty. The small concentration of RCs with ubiquinone-10 was subtracted from the total RC concentration to accurately reflect the number of available Q_A sites. The additional $RCQ^{\pm}$ found on the second flash was determined at flash intervals of 50, 100, and 200 ms. The rate of reforming the ground state from $RCQ^{\pm}$ (k_{AP}) was determined from an exponential fit to the charge recombination kinetics in RCs saturated with added quinone after subtraction of the contribution of the UQ-10-containing RCs. The signal was averaged 10 times. The data were fit with model A in the Supporting Information.

The association rate of the slower binding hydroxyl quinones was measured from the loss of DQ activity with time. The RC concentration was 1 μM with 30 μM DQ. The hydroxyl quinone concentration was varied from 7 to 300 μM. The time-dependent DQ activity was measured at 0.5 to 1.0 min intervals until equilibrium was reached and there was no additional change in the $RCQ^{\pm}$ formed by a flash.

Viscosity Dependence of k_{on}. The second-order association rate constant (k_{on}) is predicted to be inversely proportional to the solvent viscosity (eq 6) (*17*)

$$\frac{k_{on}^{\ 0}}{k_{on}^{\ v}} = A + B\frac{\eta}{\eta_0} \qquad (6)$$

k_{on}^0 and k_{on}^v are the association rate constants and η_0 and η are the solvent viscosity in the absence and presence of the viscosity modifier, respectively. A and B are fitting parameters, where $A = 0$ and $B = 1$ for an ideal in the case for an ideal diffusion-limited interaction. The solvent was modified by adding 10−60% (w/w) glycerol. The values η_0 and η were taken from the CRC Handbook of Chemistry and Physics (*18*).
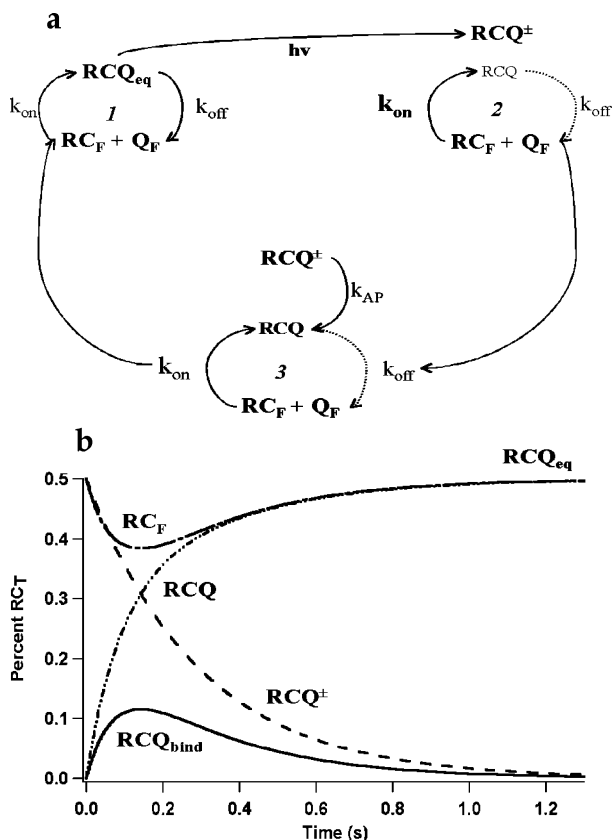
a

b

FIGURE 1: Double-flash assay used to measure the fast binding kinetics of the active neutral quinones. (a) (1) Initially, the sample is at equilibrium with $k_{on}[\text{RC}_F][\text{Q}_F] = k_{off}[\text{RCQ}_{eq}]$. [RCQ$_{eq}$] is the equilibrium concentration of RCs with bound quinone given [RC$_T$] and [Q$_T$]. (2) First flash initiates electron transfer forming the charge-separated state (RCQ$^\pm$) with semiquinone bound at the Q_A site, depleting RCQ to $(1 - \lambda)[\text{RCQ}_{eq}]$, where λ is the fraction of RCs that absorb a photon on a flash (see the Supporting Information). Now, the association rate is faster than the dissociation, $k_{on}[\text{RC}_F][\text{Q}_F] \gg k_{off}[\text{RCQ}_{eq}]$. (3) RCQ is reformed by association of RC$_F$ and Q$_F$ and by charge recombination from RCQ$^\pm$ at k_{AP}. As these two processes take place, a second flash measures the additional RCQ formed because of binding. When charge recombination is complete, the initial equilibrium concentrations are reformed (1); therefore, a second flash now generates as much RCQ$^\pm$ as the first. (b) Concentration of RC populations as a function of time given $\lambda = 1$. At the time of the first flash ($t = 0$), all RCQ$_{eq}$ is transformed into the charge-separated state (RCQ$^\pm$); thus, [RCQ] = 0 and [RCQ$^\pm$] = [RCQ$_{eq}$]. Net association of RC$_F$ and Q$_F$ yields RCQ$_{bind}$-depleting RC$_F$. Simultaneously, charge recombination reforms RCQ from RCQ$^\pm$ at k_{AP}. When charge recombination is complete, [RCQ] = [RCQ$_{eq}$], and [RCQ$^\pm$] and [RCQ$_{bind}$] = 0. A second flash monitors how [RCQ$_{bind}$] changes with time. For this simulation, the Q_A sites are 50% saturated, [RCQ$_{eq}$] = [RC$_F$] = $^1/_2$[RC$_T$], and [Q$_T$] = $^1/_2$[RC$_T$] + [K_d]. K_d = 0.6 μM, RC$_T$ = 1.0 μM, k_{on} = 8 × 10^6 M^{-1} s^{-1}, and k_{AP} = 3.5 s^{-1}.

RESULTS

Measuring Binding Kinetics of Active, Neutral Benzo- and Naphthoquinones. The association rate constants (k_{on}) were measured by a double-flash method (Figure 1). Quinone concentrations were chosen so there is a mixture of RCs with occupied (RCQ) and empty (RC$_F$) Q_A-binding sites. Because there was no indication of Q_B activity, the Q_B site is assumed to be empty. The sample starts off at equilibrium with quinone freely associating and dissociating from the protein with rates k_{on} and k_{off} (Figure 1a). The first flash forms charge-separated P$^{•+}$Q$_A$$^{•-}$ state (RCQ$^\pm$) from RCQ, depleting RCQ$_{eq}$ and leaving RC$_F$ unchanged. Because Q$_A$$^{•-}$ dissociates
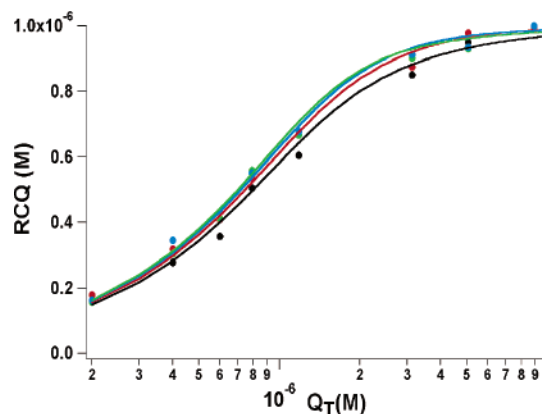

FIGURE 2: Concentration of quinone-bound RCs (RCQ = RC$_{eq}$ + RCQ$_{bind}$) as a function of the DQ concentration (Q$_T$) is plotted for the first flash (black) and at delay times for the second flash of t = 50 ms (red), t = 100 ms (green), and t = 200 ms (blue). For time t = 0, RCQ$_{bind}$ is zero (RCQ = RCQ$_{eq}$). The data are corrected for 10% residual ubiquinone-10 at Q$_A$ and for light saturation, λ, of 85%. The solid lines are solutions to model A (see the Supporting Information), with a k_{on} of 5.5 × 10^6 M^{-1} s^{-1}, K_d of 0.4 μM, and k_{AP} of 3.4 s^{-1}. Conditions: 0.93 μM RCs in 10 mM Tris at pH 7.8 and LDAO = 0.005% at room temperature.

much more slowly than Q$_A$ (*13*), the system is no longer at equilibrium. This depletion of RCQ causes association to be much faster than dissociation ($k_{on}[\text{RC}_F] \gg k_{off}[\text{RCQ}]$); thus, additional RCQ is formed, denoted RCQ$_{bind}$, which can be detected by a second actinic flash. Simultaneously, charge recombination within the RCQ$^\pm$ state reforms RCQ at k_{AP}, moving the system back toward equilibrium (see the Supporting Information for a detailed description). Once charge recombination is complete, the equilibrium concentrations are restored.

The double-flash measurements were carried out at increasing quinone concentrations (Figure 2). The second flash, delivered 50, 100, and 200 ms after the first, generates additional RCQ (RCQ$_{bind}$). The extra amplitude depends on the time delay, the quinone concentration, light saturation, and k_{AP}, all of which can be determined independently and on the association rate constant (k_{on}). The amplitude of the second flash initially increases (when association is the dominant process) and then goes back to the value of the first flash as the delay time becomes longer (Figure 1). RCQ$_{bind}$ is always small. When K_d is smaller than the RC concentration at subsaturating quinone, there is little Q$_F$ left to bind. The decay back to the ground state at k_{AP} provides a short window for observation. In addition, the subsaturating flash means that RCQ is not completely depleted on the first flash. Under conditions used here, RCQ$_{bind}$ is less than 10% of the total RCs. However, qualitatively, formation of RCQ by association between flashes can be seen in the tighter apparent affinity of RC for quinone on the second flash (Figure 2). The k_{on} yielding the set of curves that best overall fit to the concentration dependence at the three delay times is determined. Duroquinone (DQ) with a K_d of 0.40 μM and k_{AP} of 3.4 s^{-1} has a k_{on} of 5.5± 1.5 × 10^7 M^{-1} s^{-1} and a k_{off} of 3.3 s^{-1} (given $k_{off} = k_{on}K_d$). The k_{on} values for 2,3-dimethoxy-5-methyl BQ (UQ$_0$) and seven tailless 1,4-naphthoquinones range from 10^5−10^7 M^{-1} s^{-1}, while k_{off} varies from 0.2 to 6 s^{-1} (Table 1).

Measuring Binding Kinetics for Inactive, Anionic Hydroxyl Naphthoquinones. The pK_a values for the hydroxyl quinones

Table 1: Binding Rates and Affinities for Neutral Quinones at the Q_A Site of RCs

a	quinone	K_d (μM)[b]	$k_{on} \times 10^{-6}$ ($M^{-1} s^{-1}$)[c]	k_{off} (s^{-1})[d]	k_{AP} (s^{-1})[e]
1	UQ$_0$	86 ± 16	0.07 ± 0.01	6.0	10
2	1,2-NQ	13 ± 3.0	0.07 ± 0.06	0.9	8.3
3	1,4-NQ	7.4 ± 1.2	0.6 ± 0.03	0.6	7.1
4	2-MeOx-NQ	0.5 ± 0.1	0.3 ± 0.1	0.2	12
5	2-Me-NQ	0.6 ± 0.1	2.6 ± 1.0	1.6	7.4
6	DQ	0.4 ± 0.1	5.5 ± 1.5	3.3	3.4
7	2,3-dMe-NQ	0.1 ± 0.02	9.4 ± 3.0	1.3	6.7
8	2-Br-NQ	0.2 ± 0.02	4.8 ± 3.0	0.9	3.3

[a] Numbers are used as labels in Figure 8. [b] K_d was obtained from the amount of RCQ$^\pm$ formed after a single flash as a function of the concentration of added quinone (eq 1). [c] k_{on} was measured with the double flash assay (as shown for DQ, Figure 2). [d] k_{off} is derived from $K_d = k_{off}/k_{on}$. [e] k_{AP} is the $Q_A^{\bullet-}$ to $P^{\bullet+}$ charge recombination rate constant.

range from 4.0 to 9.4 (Table 2). Above their pK_a, none of these quinones reconstitutes Q_A function. Their binding is measured by their competition with the active DQ. The K_I values, at pH values above their pK_a values, vary from 0.04 to 5 μM. The neutral 5-OH-2-Me-NQ does bind rapidly and will reconstitute Q_A activity (manuscript in preparation). Measurement of the association of neutral 5-OH-2-Me-NQ is complicated because the Q_A site downshifts the pK_a; therefore, the bound quinone is not fully protonated even at pH 7.2.

The pK_a of 5-OH-2-Me-NQ is 9.4. At pH 10.2, the ionized species is a competitive inhibitor at the Q_A site. Its slow association rate was determined from the time-dependent loss of DQ activity (Figure 3a). In a sample with 70−80% of the Q_A sites occupied by DQ, 90−300 μM 5-OH-2-Me-NQ was added. Activity is lost as DQ is displaced from the Q_A site with the system reaching equilibrium in 6−10 min (Figure 3a). The dependence of the equilibrium DQ activity on the inhibitor concentration provides a K_I of 5 ± 3 μM (Table 2). To determine the reversibility of binding, the dissociation rate constant, k_{off}, was measured directly from the time-dependent increase of activity when DQ added to a sample is pre-equilibrated with the hydroxyl quinone. Ionized 5-OH-2-Me NQ displays completely reversible binding with a k_{off} of 1.7×10^{-4} s^{-1} (Figure 3b).

Determination of the Binding Mechanism. The anionic hydroxyl quinones bind in minutes, much slower than the $10^6–10^9$ s^{-1} expected for a diffusion-dominated process. They bind at least 1000 times slower than the neutral quinones with comparable K_d values (Tables 1 and 2). The quinone concentration dependence of the rate constants can clarify whether the rate-limiting step is first or second order. For a second-order rate-determining step, the association rate
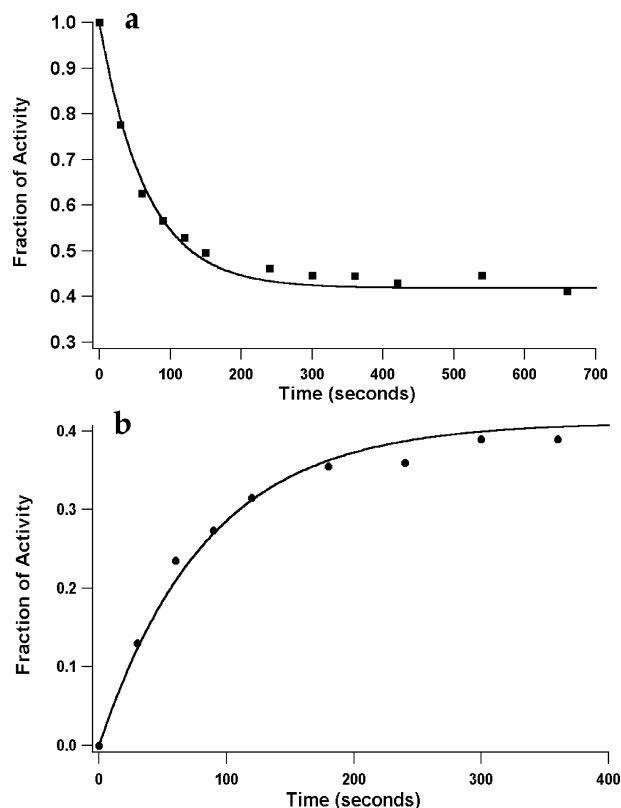
FIGURE 3: Time dependence of DQ-dependent activity in the presence of 5-OH-2-Me NQ at pH 10.2. (a) Loss of activity following the addition of 160 μM 5-OH-2-Me NQ at $t = 0$ to 1 μM RCs with 30 μM DQ. The line is the best fit to the first-order binding model E (see the Supporting Information) with a k_{uni} of 1.7×10^{-2} s^{-1}. (b) Restoration of DQ-dependent activity following the addition of 30 μM DQ to 1 μM RCs preincubated with 160 μM 5-OH-2-Me NQ for 30 min at pH 10.2. The solid line is the best fit to model C (see the Supporting Information) with a k_{off} of 2.0×10^{-4} s^{-1}.

constant k_{on} (M^{-1} s^{-1}) is independent of the quinone concentration, while the apparent first-order rate constant k_{uni} (s^{-1}) is a linear function of the concentration with $k_{uni} = k_{on}[Q_T] + k_{off}$ (20). On the other hand, for a first-order rate-determining step, k_{uni} (s^{-1}) is independent of the quinone concentration, while the apparent k_{on} (M^{-1} s^{-1}) is a reciprocal function of the concentration, $k_{on} = A + k_{uni}/[Q_T]$, where A is the observed second-order rate constant at a saturating quinone concentration.

Concentration Dependence of the Neutral Quinones Association Rate. For the active fast binding neutral quinones, the change in second flash amplitude at three different delay times at a single quinone concentration was fit to a second-order model (A in the Supporting Information), providing

Table 2: Binding Rates and Affinities for Anionic Hydroxyl Quinone at the Q_A Site of RCs

a	quinone	pH[b]	K_I[c] (μM)	$k_{uni} \times 10^2$ (s^{-1})	$k_{off} \times 10^4$ (s^{-1})	pK_a	wavelength[d] (nm)
9	2-OH-NQ	7.8	0.1 ± 0.05	7.0 ± 2.0[e]	3 ± 0.7	4.16	540
10	5-OH-NQ	10.2	0.6 ± 0.2	2.2 ± 0.2	1 ± 0.5	9.12	530
11	2-OH-3-Iso-NQ	10.2	4.0 ± 2.3	0.7 ± 0.1	2 ± 0.3	5.85	480
12	5-OH-2-Me-NQ	10.2	4.5 ± 1.4	1.7 ± 0.7	2 ± 0.6	9.4	520
	2-OH-3-Me-NQ	7.8	ND[f]	0.5 ± 0	ND	5.15	480

[a] Numbers are used as labels in Figure 8. [b] K_I values and first-order association and dissociation rate constants measured at a pH above the hydroxyl group pK_a. [c] K_I is obtained from the concentration dependence of the equilibrium DQ activity on the inhibitor concentration. [d] Wavelength used to measure absorbance difference between neutral and ionized hydroxyl quinone to determine the pK_a in aqueous solution. [e] Measured above 25 μM, where k_{on} is independent of the quinone concentration (Figure 5). [f] ND, dissociation of 2-OH-3-Me could not be detected (Figure 6).
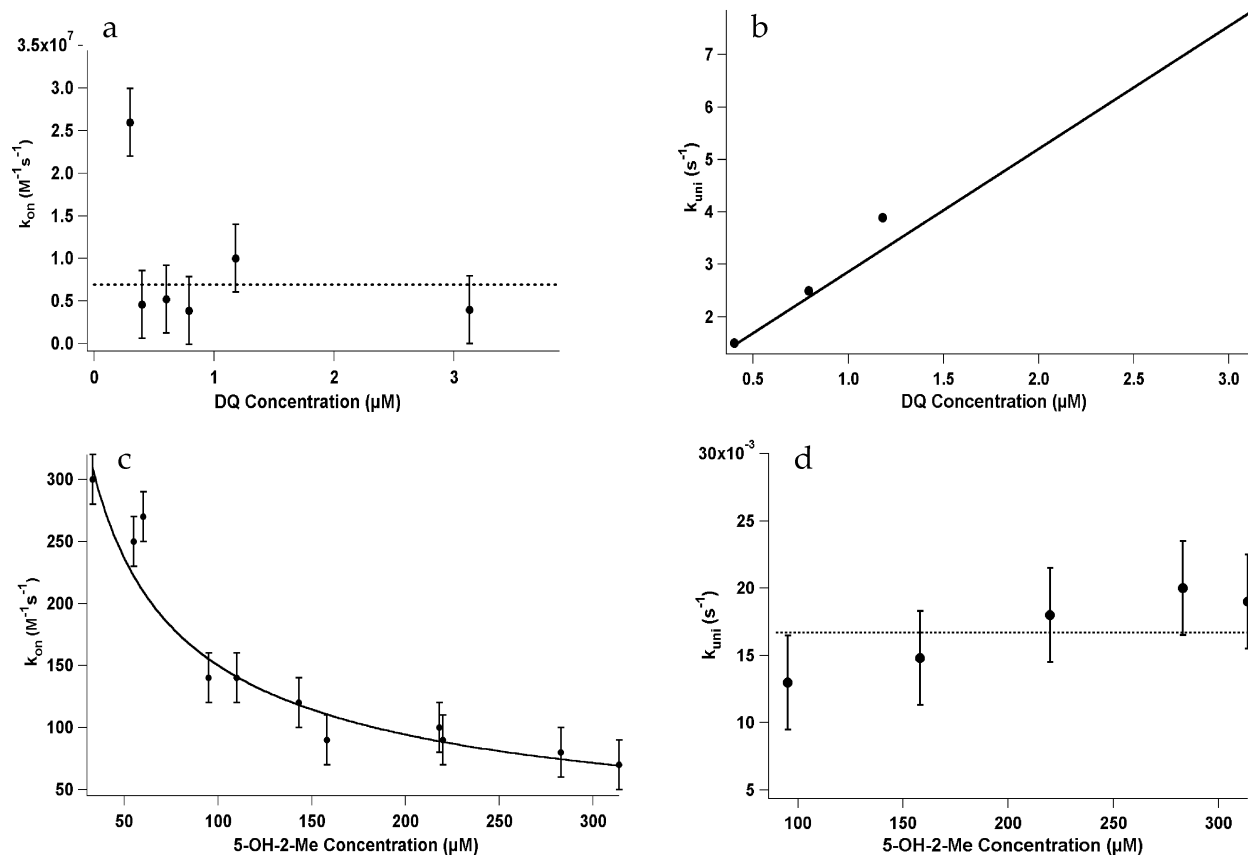
FIGURE 4: Dependence of the derived first- and second-order rate constants (k_{uni} and k_{on}) on the quinone concentration. (a–b) DQ, a neutral quinone. The DQ concentrations tested yield 30−85% saturation of Q_A-binding sites. (a) Concentration dependence of the second-order association rate constant. k_{on} was derived by fitting the double-flash data at the three delay times (50, 100, and 200 ms) at the given quinone concentration (A in the Supporting Information). The dashed line is 6.9×10^6 M^{-1} s^{-1}, which is the mean value of six fits. (b) Fit of the data with the first-order model (D in the Supporting Information) provided k_{uni}. The solid line is the best fit obtained by linear regression with slope $= 2.4 \times 10^6$ M^{-1} s^{-1} and y intercept $= 0.52$ s^{-1}. The experimental conditions are 1 μM RCs in 10 mM Tris and 0.005% LDAO at pH 7.8. (c−d) 5-OH-2-Me-NQ, an anionic quinone inhibitor. (c) Second-order rate constant (k_{on}) (B in the Supporting Information) displays a reciprocal concentration dependence, as expected for a first-order rate-determining step. The solid line is k_{on} (M^{-1} s^{-1}) $= 26 + 0.008/[Q_T]$. (d) First-order rate constant (k_{uni}) (E in the Supporting Information) is independent of the hydroxyl quinone concentration. The dashed line at 0.017 s^{-1} is the average k_{uni} for all of the measurements. The experimental conditions are 1 μM RCs in 10 mM CAPS and 0.005% LDAO at pH 10.2.

k_{on}, and with a first-order model (D in the Supporting Information), providing k_{uni}. The k_{on} for DQ measured in this way gives a mean value of 6.9×10^6 M^{-1} s^{-1} (Figure 4a) in reasonable agreement with 5.5×10^6 M^{-1} s^{-1} found by a global fit of the data (Figure 2). The neutral quinone k_{on} values are concentration-independent, as shown for DQ (Figure 4a), indicating a second-order rate-determining step. As expected, k_{uni} is a linear function of the quinone concentration. The slope of the concentration dependence of k_{uni} for DQ is 2.4×10^6 M^{-1} s^{-1} (Figure 4b), which is in reasonable agreement with the measured k_{on} (Figure 2). The y intercept (Figure 4b) is not in good agreement with the k_{off} obtained from $K_d k_{on}$ (Table 1). For example, 2-Me-NQ has a negative y intercept (data not shown). However, it is not unusual that this method of analysis does not usually provide accurate values for k_{off} (20).

Concentration Dependence of the Hydroxyl Quinone Association Rate. The association data for the slow binding anionic hydroxyl quinones (Figure 3) was fit with a second-order model (B in the Supporting Information) providing k_{on} and with a first-order model (E in the Supporting Information) providing k_{uni}. 5-OH-NQ and 5-OH-2-Me-NQ show a first-order rate-determining step. For 5-OH-2-Me-NQ, k_{uni} is concentration-independent (Figure 4d) with the average

value of 0.017 s^{-1}, while k_{on} depends on $[Q_T]^{-1}$ (Figure 4c). The k_{uni} derived from fitting the concentration dependence of the observed second-order rate (k_{on}) is 0.008 s^{-1} in reasonable agreement with the directly determined value.

Both 5-OH quinones show completely reversible binding that is consistent with a first-order rate-determining step. Thus, k_{on} can be determined by the loss of activity after the quinone is added to RCs reconstituted with DQ (Figure 3a), while k_{off} can be determined from the restoration of activity when DQ is added to RCs preincubated with the hydroxyl quinone (Figure 3b). The same K_I is derived from the concentration dependence of the long time asymptote found in both measurements and is consistent with the value determined from k_{uni}/k_{off}.

The three quinones with an orthohydroxyl group present data that is more difficult to interpret. The apparent second-order rate constant (k_{on}^{obs}) for 2-OH-NQ fits a model similar to 5-OH-2-Me-NQ (Figure 4c) with $k_{on}^{obs} = 900$ M^{-1} s^{-1} + 0.05 s^{-1}/[Q_T] (Figure 5a), suggesting that the rate-determining step is first-order. On the other hand, the observed rate (k_{uni}^{obs}) of 2-OH-NQ is quinone concentration-dependent at low concentrations, becoming independent at higher concentrations (Figure 5b). This indicates that the rate-determin-
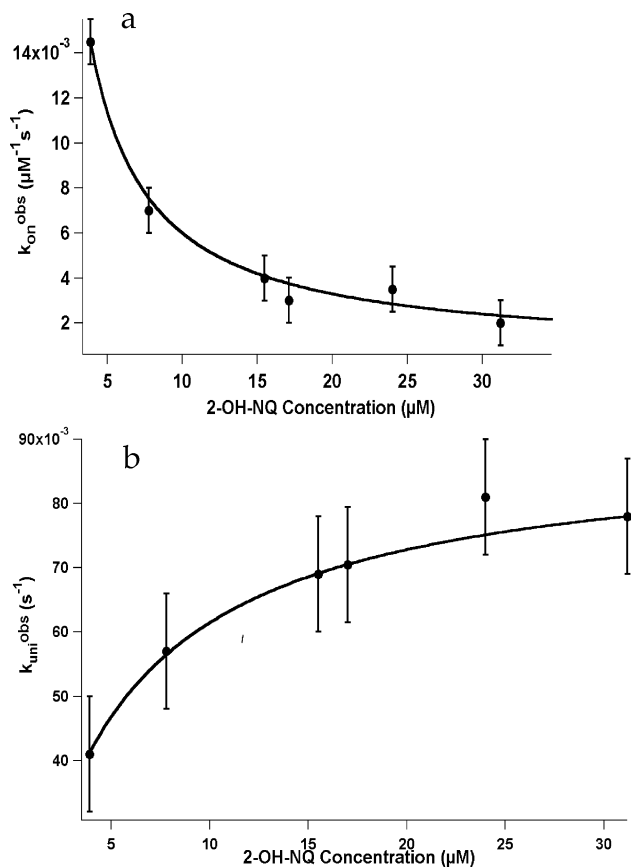
FIGURE 5: (a) Concentration dependence of second-order rate constant (k_{on}) for 2-OH-NQ. The solid line is the best fit curve, $k_{on}^{obs} = 900$ M^{-1} s^{-1} + 0.05/[Q$_T$]. (b) Concentration dependence of first-order rate constant (k_{uni}) for 2-OH-NQ. The solid line is k_{uni}^{obs} = 0.089 s^{-1}/(1 + 4.5/[Q$_T$]). The experimental conditions are 1 μM RCs in 10 mM Tris and 0.005% LDAO at pH 7.8.

ing step itself is concentration-dependent. Thus, the rate was treated with a model consisting of two barriers; one is first-order, and the other is second-order (their sequence is unspecified) (21). At low concentrations, the second-order association process limits the rate, with k_{uni}^{obs} being concentration-dependent (Figure 5b). However, the reaction cannot proceed faster then the first-order step, which is rate-limiting at high concentrations. Thus, $k_{uni}^{obs} = k_{uni}/(1 + K_{bi}/[Q_T])$, where k_{uni} is the true rate constant for the first-order step and K_{bi} is the dissociation constant for the second-order process (Figure 5b). Fitting the data to this model yields k_{uni} = 0.089 s^{-1}, comparable to the values found for the other anionic quinones, and K_{bi} = 4.5 μM. The affinity of the initial encounter is significantly weaker then the overall K_d of 0.1 μM (Table 2), indicating that protein conformational changes in the subsequent first-order step may tighten binding. There is reasonable agreement between the k_{uni} obtained from concentration dependence of the rate (0.089 s^{-1}) and from the apparent second-order model (0.05 s^{-1}) (Figure 5).

If DQ is added to a sample pre-equilibrated with an anionic hydroxyl quinone, full activity can be recovered with 2-OH-NQ, 5-OH-NQ, and 5-OH-2-Me-NQ (Figure 3B). For these quinones, the directly measured k_{off} matches the value derived from $k_{on}K_I$. However, for 2-OH-3-Me-NQ, the addition of DQ does not restore any activity (Figure 6). This is consistent with K_I being in the subnanomolar range.

There are no changes in RC spectra that would indicate significant changes in the structure because of incubation
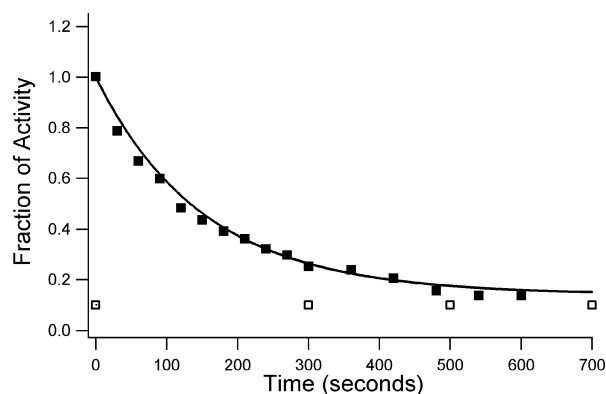

FIGURE 6: Binding of 2-OH-3-Me. (■) At $t = 0$, 23 μM of 2-OH-3-Me was added to 30 μM DQ equilibrated with 1 μM RC$_T$ (pH 7.8). The time course for the inhibition of DQ activity yielded the measured k_{uni} of 8×10 s^{-1}. (□) 30 μM DQ is added to a sample with 1 μM RC$_T$ pre-equilibrated for 30 min with 23 μM 2-OH-3-Me (in 10 mM Tris at pH 7.8). No DQ activity was detected.

with 2-OH-3-Me-NQ. Similar measurements with 2-OH-3-Iso-NQ show that only 50% of the activity is recovered and k_{off} is slower than $k_{on}K_I$, indicating that the dissociation mechanism is not just the reverse of association.

Viscosity Dependence of k_{on}. For a second-order rate-determining step, diffusion plays a dominant role; thus, the rate constant is predicted to be inversely proportional to the solvent viscosity (η) (22). Using glycerol as a solvent modifier, the viscosity dependence of k_{on} for DQ and 2-Me-NQ was determined (Figure 7a). The dashed lines represent the ideal diffusion controlled reaction, where the product $k_{on}\eta$ is constant (eq 6). The k_{on} values for these two neutral quinones have strong viscosity dependence (Figure 7a), consistent with a second-order rate-determining step. For DQ, the association rate becomes slower than expected as the viscosity increases, because k_{on} is above the dashed line in Figure 7a. The reason for this is not clear, but it may be due to solvent osmotic pressure, which has been observed previously when glycerol is used as a solvent modifier (17). On the other hand, the second-order rate constants (k_{on}) for the anionic 5-OH-2-Me-NQ and 2-OH-NQ are independent of viscosity (Figure 7b), supporting a first-order rate-determining step for the hydroxyl–quinones.

Ionic Strength Dependence of k_{on} and k_{uni}. Binding kinetics were measured at NaCl concentrations of 0–300 mM. Ionic strength will affect the binding rate if electrostatic interactions between RCs and quinone are important for the rate-determining step. Neither k_{on}, for the neutral quinones, nor k_{uni}, for the anionic quinones, depend on the ionic strength (data not shown). Thus, electrostatic interactions do not govern the rate-determining step. For the hydroxyl quinones, this is further evidence of a first-order rate-determining step because solution counterions would be expected to shield electrostatic interactions between the anionic inhibitor and the RCs.

Comparing Binding Rates and Equilibrium Affinity. The K_d values for the fast binding neutral quinones and the K_I values for the slow binding hydroxyls are in the same range (0.1–90 μM), yet their dissociation rates differ by 10^3–10^4-fold (Figure 8a). For the neutral quinones, the association rate (k_{on}) correlates with K_d; thus, an increase in binding strength is predominately due to faster association (Figure 8b). 2-MeOx-NQ deviates from this trend because its k_{on} is
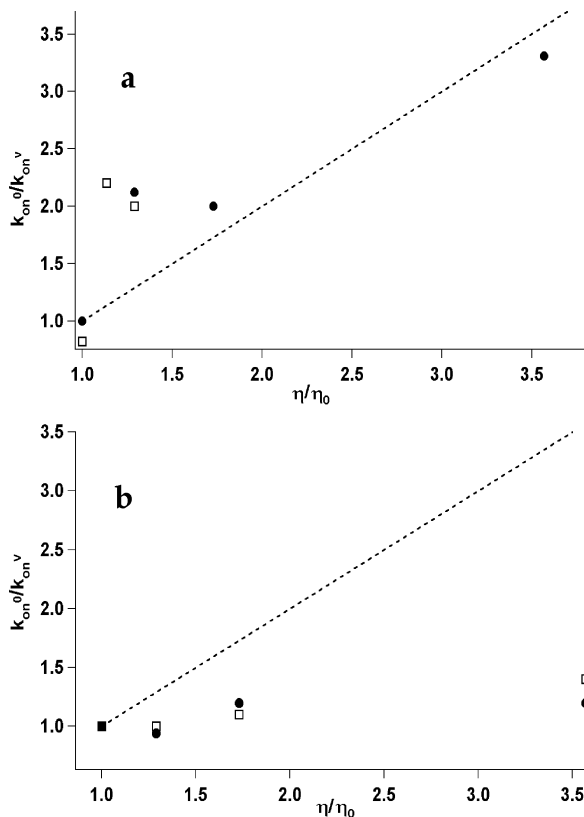
FIGURE 7: Viscosity dependence of the second-order association rate constant (k_{on}). The dashed line has a slope of 1 representing the expected trend for a second-order diffusion-controlled association reaction (eq 6). Each data point represents the average k_{on} measured with 1 μM RC in 0.005% LDAO at 20, 50, and 70% binding saturation for each quinone. (a) $\square$, DQ; and $\bullet$, 2-Me-NQ measured in 10 mM Tris at pH 7.8. (b) $\square$, 5-OH-2-Me-NQ (measured in 10 mM CAPS at pH 10.2); and $\bullet$, 2-OH-3-Me-NQ (measured in 10 mM Tris at pH 7.8).

slower than expected given its K_d. Methoxy substituents lower the quinone partition coefficient, preferring the aqueous phase, which can increase the energy barrier for association (*9*). The Q_A site interacts strongly with the methoxy group, keeping the K_d tight despite the association barrier.

DISCUSSION

The comparison of binding neutral and anionic quinones to the Q_A site of RCs show that the negatively charged hydroxyl quinones dissociate about 10^4 times more slowly than neutral quinones with comparable K_d values (Figure 8a). In addition, these quinones have different mechanisms for binding. The linear dependence of the apparent first-order rate constant (k_{uni}) on the quinone concentration shows that the rate-determining step for the neutral quinones is second order (Figure 4) (*17, 23, 24*). The dependence of K_d on the second-order k_{on} shows that the association rate plays the dominant role in controlling affinity (Figure 8). The solvent viscosity dependence indicates this is a primarily diffusion-controlled process (Figure 7). The measured rate constants of these quinones (10^5-10^7 M^{-1} s^{-1}) are typical of the association of large proteins with small ligands, where only a small fraction of the protein surface can form an active encounter complex (*25, 26*).

The anionic hydroxyl quinones are slow binding inhibitors at the Q_A site. In addition to binding tightly, many transition-
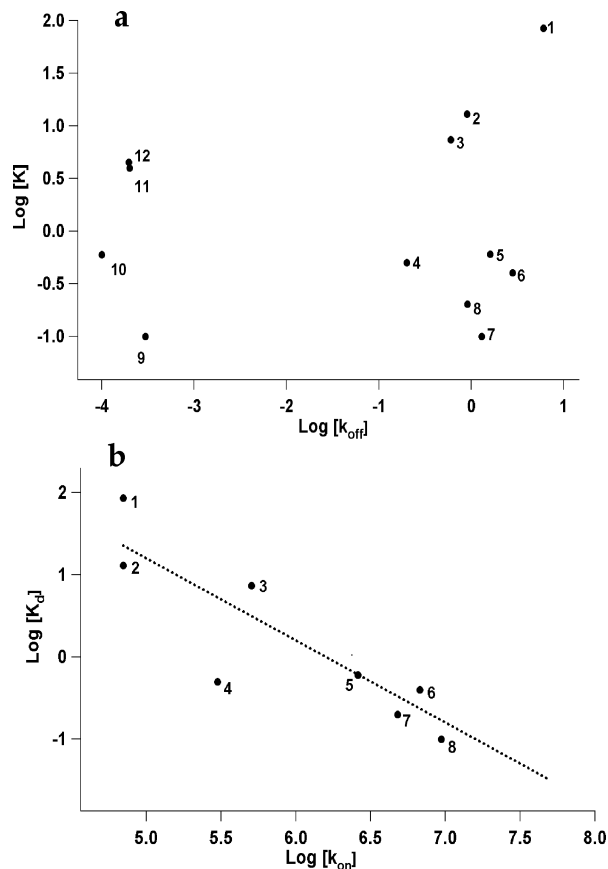

FIGURE 8: Binding affinity versus binding rate constants for neutral and anionic quinones. (a) Comparison of the dissociation rate (k_{off}, s^{-1}) and the binding affinity (K is K_d for neutral quinones and K_I for hydroxyl quinones in units of micromolars). The anionic hydroxyl quinones (9–11) dissociate about 10 000-fold more slowly than neutral quinones (1–8) with comparable K_d values. (b) Comparison of the second-order association rate (k_{on}, M^{-1} s^{-1}) and the binding affinity (K_d, μM) for the neutral quinones. The dashed line has a slope of -1 showing the correlation between $\log(K_d)$ and $-\log(k_{on})$. The quinone labels from Tables 1 and 2. 1, UQ$_0$; 2, 1,2-NQ; 3, 1,4-NQ; 4, 2-MeOx-NQ; 5, 2-Me-NQ; 6, DQ; 7, 2,3-diMe-NQ; 8, 2-Br-NQ; 9, 2-OH-NQ; 10, 5-OH-NQ; 11, 2-OH-3-Iso-NQ; and 12, 5-OH-2-Me-NQ.

state analogues bind slowly, indicating that there are large barriers for binding these high-energy reaction intermediates (*27–33*). While slow kinetics has been observed in systems with a single-step, second-order association mechanism (*30, 31*), this is not a good description of the association of anionic hydroxyl quinones with the Q_A site. The concentration independence of k_{uni} (Figure 4) and solvent viscosity independence of the second-order rate constant k_{on} (Figure 7) supports a first-order rate-determining step for these quinones. This requires a two-step binding process, for which there are two possible paths (Scheme 1). In one (P$_1$), unbound reaction centers exist in an equilibrium mixture of RC$_F$ and RC$_F^*$. RC$_F^*$, which has very low equilibrium occupancy binds rapidly and tightly to the anionic inhibitor, I$_F^-$. Here, the rate-determining step is the slow conformational change from RC$_F$ to RC$_F^*$. Along P$_2$, an initial encounter complex, RCI$^-$, is formed rapidly. This is followed by the slow change from RCI to RCI^{-*}, the more thermodynamically stable complex. The RCI complex samples many conformational states until the one that can best stabilize the anion is found. Protein rearrangement as the source of slow binding kinetics is commonly observed for enzyme inhibition (*34, 35*). Both

Scheme 1:   Two Pathways (P₁ and P₂) for the Binding of Anionic Hydroxyl Quinones with a Slow First-Order Rate-Determining Step (k_{uni})[a]
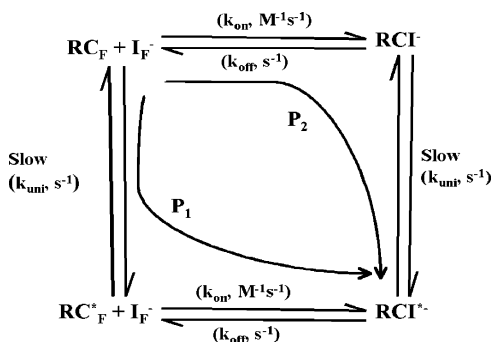
[a] The fast, reversible binding process is governed by the second-order rate constant k_{on}.

pathways have been found in studies of other proteins (*27, 35*). In either case, the measured K_d values reflect the overall affinity for formation of RCI⁻* from RC_F and I₋F.

The quinone concentration and solvent viscosity dependence of the rate establish the order of the rate-determining step but cannot distinguish between P₁ and P₂. However, the correlation between k_{uni}, k_{off}, and K_d can provide some clues. P₂ should show an initial burst phase of inhibition because of the rapid formation of RCI⁻ before the slow isomerization to form RCI⁻*. This is not observed but cannot be ruled out given the difficulty of obtaining early time measurements. The amplitude of the burst would be dependent on the affinity of I⁻ for RC_F, which may be low. Along P₁, the slow conformational rearrangements only involve RC_F. Here, the anionic hydroxyl quinones bind rapidly to the high-energy configuration (RC_F*). Because RC_F* has a low equilibrium occupancy, the overall association rate is slow. The inhibitor affinity depends on the rate at which the RCI*⁻ changes back to the low-affinity RCI⁻. A similar mechanism was used to describe the results for the slow-onset inhibition of yeast AMP deaminase (*27*).

The binding of 5-OH-NQ and 5-OH-3-Me-NQ show a first-order rate-determining step, indicating that quinone association is too fast to be observed. On the other hand, the binding of 2-OH-NQ shows kinetic evidence for both steps in formation of RCI⁻*. Here, the second-order process is rate-limiting at low quinone concentrations, while the first-order process becomes rate-limiting at higher concentrations (Figure 5).

2-OH-3-Me binds irreversibly to the Q_A site (Figure 6). Slow irreversible binding could imply the formation of a covalent bond in the active site (*36*) or that the encounter complex denatures at a rate faster than dissociation. No change in the RC near-IR absorbance spectra is found after incubation with this quinone; thus, denaturation is unlikely. The observed irreversible binding could also indicate that the affinity is in the subnanomolar range. Adding a methyl group at the 3 position would need to increase the affinity of 2-OH-NQ ($K_I = 0.1$ μM) by at least 100-fold to keep DQ from displacing it under the experimental conditions employed here. The neutral diortho-substituted 2,3-dMe-NQ does bind ≈6-fold more tightly than the monosubstituted 2-Me-NQ (Table 1), showing that the addition of an orthomethyl group tightens binding. In contrast, 2-OH-3-Iso-NQ ($K_I = 4.2$ μM) binds more weakly than the

monosubstituted 2-OH−NQ (Table 2). However, it is likely that the branched isopropyl group weakens affinity (Gunner, unpublished results). Continuum electrostatic calculations do indicate that ionized 2-OH-3-Me-NQ binds 40-fold tighter than 2-OH-NQ (manuscript in preparation).

Anionic Hydroxyl Quinones as Models for the Semiquinone. Previous studies of difference FTIR (*37, 38*), electrochromatic shifts following Q_A⁻ formation (*39*), E_m shifts in replacement compounds (*40*), and mutational analysis (*41, 42*) indicate that it is the negative charge on the quinone that causes the protein response following formation of Q_A⁻. Thus, even though the anionic hydroxyl quinones are not radicals, they can serve as models for the study of semiquinone binding. The results presented here show that a negative charge causes slow binding kinetics at the Q_A site. At pH 7.8, neutral 5-OH-2-Me-NQ with a pK_a of 9.4 is a fast binding neutral compound that can reconstitute Q_A activity (manuscript in preparation), while at high pH, the anionic quinone dissociates slowly. Semiquinones dissociate slowly from the Q_A and Q_B sites (*14*). Ferrocene, an external electron donor of P⁺, creates RCs in the state PQ_A⁻. For a number of tailless semiquinones in the Q_A site, this state is trapped for seconds (*13*). Semiquinone disappearance was attributed to the accessibility of external oxidants, and preliminary results indicate that in O₂-depleted samples the semiquinone lifetime increases (data not shown). These results put an upper limit on semiquinone k_{off} of 0.5 s⁻¹ for DQ⁻, 1000-fold faster than the anionic hydroxyl quinones but 10-fold slower than the neutral DQ (Table 1). Thus, the slower dissociation of the hydroxyl quinones could provide a better limit for the semiquinone lifetime in the absence of external oxidants.

The observed rate of anionic hydroxyl quinone binding is slow. Physiologically, slow conformational changes cannot be required for formation of the Q_A⁻, which accepts an electron from bacteriopheophytin in 150 ps (*43*). However, relaxation stabilizes the RCQ± charge-separated state once it is formed (*44−48*). Events such as proton uptake, internal charge transfer, and the reorganization of internal dipoles have been proposed to stabilize Q_A⁻ (*49−51*). Furthermore, changes in a cluster of acidic residues near the Q_B site help stabilize Q_A⁻ (*52, 53*), perhaps though shifts in their ionization (*50*).

The relative affinity of quinone and semiquinone for the Q_A site determines how the *in situ* E_m differs from that found in solution (Figure 9). While it is difficult to measure E_m values for single-electron reductions of quinone in water, some have been estimated (*9, 54, 55*). The $E_{m,sol}$ for UQ/UQ⁻ is ≈ −145 mV (*4, 56, 57*), while it is −45 (*58*) to −75 mV (*59*) in the Q_A site at pH 7. This 70−100 mV E_m shift indicates the semiquinone binds 15−45 times more tightly than the quinone. Inhibitor binding at the Q_B site also shows that the semiquinone binds more tightly than the quinone or dihydroquinone (*14*). The work presented here allows for the comparison of the relative affinity of neutral and anionic quinones. The k_{off} values for the anionic hydroxyl quinones are 10⁴ times slower than the neutral compounds (Figure 8a). If the semiquinone off rate slowed this much with no change in association kinetics, this would correspond to an E_m shift of +240 mV. However, the results presented here show that anionic compounds also associate slowly. The anionic hydroxyl and neutral quinones have different binding
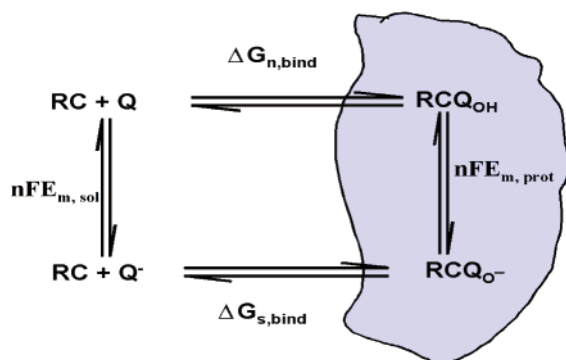
FIGURE 9: Relationship between quinone-binding energy and redox midpoint potential. $\Delta G_{s,bind}$ and $\Delta G_{n,bind}$ are the association free energies for the semiquinone and neutral quinone. $nFE_{m,prot}$ and $nFE_{m,sol}$ are the free energies for semiquinone formation in the protein and in aqueous solution, where n is the number of electrons transferred (here, $n = 1$) and F is Faraday's constant. $\Delta G_{s,bind} = nRT \log(k_{on,semi}/k_{off,semi}) = \Delta G_{n,bind} - nF(E_{m,prot} - E_{m,sol})$.

mechanisms; therefore, their association rate constants cannot be directly compared. However, a comparison of the rate of formation of the bound complex at 50% saturation shows that the average k_{on} for the neutral quinones is in the range of 10^6-10^7 M^{-1} s^{-1} (Table 1), while, using 5-OH-2-Me-NQ as an example, $k_{uni}/[Q_T]$ is 3500–5500 M^{-1} s^{-1}. Thus, the anionic quinones associate 180–2800 times more slowly, while k_{off} slows by 10^4 compared to the neutral quinones. Assuming the same shift in the binding kinetics of the quinone and semiquinone predicts a ~33–100 mV increase in E_m, in good agreement with the measured E_m shift. Because there is no free semiquinone in either membrane or solution, slow semiquinone association would not affect RC activity. The slow k_{off} helps preserve the unstable, high-energy semiquinone $Q_A^{\bullet-}$, minimizing energy loss and free-radical damage. This analysis assumes that all anionic quinones are stabilized by the same amount. The E_m shift moving from the aprotic solvent dimethylformamide (60) to the Q_A site is not the same for all compounds, indicating that specific protein interactions can also play an important role (10, 40).

The measured K_d values for the neutral and anionic hydroxyl quinone (Tables 1 and 2) reflect the free-energy difference of the quinone in solution and in the Q_A site. There is a loss of solvation energy incurred by transferring the quinone from the high dielectric environment of water ($\epsilon = 80$) into the low dielectric protein and loss of motional degrees of freedom in the binding site (4). Charged compounds interact with water more favorably than neutral ones. Thus, the anionic hydroxyl quinones need to have additional favorable interactions with the protein to have K_d values that are similar to the neutral quinones. The partition coefficient (P) provides a quantitative measure of the energy of transferring the quinone out of water and into a noninteracting solvent such as cyclohexane ($\Delta G_{trans} = 2.3RT \log P$) (61). While some neutral quinones have measured partition coefficients (9, 62), anionic quinones do not. The difference in the partition coefficient ($\Delta \log P$) of ionized and neutral forms of 5-OH-NQ in octanol was estimated with a fragment-based method (www.molinspiration.com) (63, 64). Octanol is a more polar solvent than cyclohexane; thus, this provides a lower limit of the free energy for transferring the anionic quinone from water. The $\Delta \log P$ was 2.2 corresponding to

a $\Delta\Delta G_{trans}$ of -3 kcal/mol (130 meV). Previous electrostatic calculations have shown that the protein interacts -2.5 kcal/mol more favorably with $Q_A^{\bullet-}$ compared to Q_A, corresponding to a 72-fold tighter K_d favoring anion binding (4). Favorable interactions with protein side chains, the backbone dipoles, and the non-heme iron were found to stabilize anion binding.

Anthraquinone (AQ) and substituted derivatives have smaller E_m shifts from solution values in the Q_A site than benzo- and naphthoquinones (10). These semiquinones should therefore be more weakly bound relative to the neutral quinone and could show faster dissociation rates. Preliminary results using the double-flash method with 1-Cl-AQ and 2-Cl-AQ showed that the amplitude decreases rather than increases on the second flash, consistent with semiquinone dissociating between flashes. These low-potential quinones have fast charge recombination kinetics making it difficult to model the binding kinetics on the same time scale as the other neutral quinones in this study.

ACKNOWLEDGMENT

SUPPORTING INFORMATION AVAILABLE

Mathematical model for the double-flash method (model A), including the corrections made for light saturation and the mathematical models for all other binding models (B–E). This information is available free of charge via the Internet at http://pubs.acs.org.

REFERENCES

1. Stowell, M. H. B., McPhillips, T. M., Rees, D. C., Soltis, S. M., Abresch, E., and Feher, G. (1997) Light-induced structural changes in photosynthetic reaction center: Implications for mechanism of electron–proton transfer, *Science 276*, 812–816.
2. Kirmaier, C., and Holten, D. (1993) in *The Photosynthetic Reaction Center* (Deisenhofer, J., and Norris, J. R., Eds.) pp 49–70, Academic Press, San Diego, CA.
3. Gunner, M. R. (1991) The reaction center protein from purple bacteria: Structure and function, *Curr. Top. Bioenerg. 16*, 319–367.
4. Zhu, Z., and Gunner, M. R. (2005) Energetics of quinone-dependent electron and proton transfers in *Rhodobacter sphaeroides* photosynthetic reaction centers, *Biochemistry 44*, 82–96.
5. Wraight, C. A. (2004) Proton and electron transfer in the acceptor quinone complex of photosynthetic reaction centers from *Rhodobacter sphaeroides*, *Front. Biosci. 9*, 309–337.
6. Okamura, M. Y., and Feher, G. (1995) in *Anoxygenic Photosynthetic Bacteria* (Blankenship, R., Madigan, M., and Bauer, C., Eds.) pp 577–593, Kluwer Academic Publishers, Dordrecht, The Netherlands.
7. Graige, M. S., Paddock, M. L., Bruce, J. M., Feher, G., and Okamura, M. Y. (1996) Mechanism of proton-coupled electron transfer for quinone (Q_B) reduction in reaction centers of *Rb. sphaeroides*, *J. Am. Chem. Soc. 118*, 9005–9016.
8. McPherson, P. H., Okamura, M. Y., and Feher, G. (1990) Electron transfer from the reaction center of *Rb. sphaeroides* to the quinone pool: Doubly reduced Q_B leaves the reaction center, *Biochim. Biophys. Acta 1016*, 289–292.

9. Rich, P. R., and Bendall, D. S. (1979) A mechanism for the reduction of cytochromes by quinols in solution and its relevance to biological electron transfer reactions, *FEBS Lett. 105*, 189−194.

10. Woodbury, N. W., Parson, W. W., Gunner, M. R., Prince, R. C., and Dutton, P. L. (1986) Radical-pair energetics and decay mechanisms in reaction center containing anthraquinones or benzoquinones in place of ubiquinone, *Biochim. Biophys. Acta 851*, 6−22.

11. Warncke, K., and Dutton, P. L. (1993) Influence of QA site redox cofactor structure on equilibrium binding, *in situ* electrochemistry, and electron-transfer performance in the photosynthetic reaction center protein, *Biochemistry 32*, 4769−4779.

12. Ishikita, H., Morra, G., and Knapp, E. W. (2003) Redox potential of quinones in photosynthetic reaction centers from *Rhodobacter sphaeroides*: Dependence on protonation of Glu-L212 and Asp-L213, *Biochemistry 42*, 3882−3892.

13. Kalman, L., and Maroti, P. (1994) Stabilization of reduced primary quinone by proton uptake in reaction centers of *Rhodobacter spaeroides*, *Biochemistry 33*, 9237−9244.

14. Diner, B. A., Schenck, C. C., and DeVitry, C. (1984) Effect of inhibitors, redox state, and isoprenoid chain length on the affinity of ubiquinone for the secondary acceptor binding site in the reaction centers of photosynthetic bacteria, *Biochim. Biophys. Acta 766*, 9−20.

15. Goldsmith, J. O., and Boxer, S. G. (1996) Rapid isolation of bacteria photosynthetic reaction centers with an engineered poly-histidine tag, *Biochim. Biophys. Acta 1276*, 171−175.

16. Okamura, M. Y., Isaacson, R. A., and Feher, G. (1975) The primary acceptor in bacterial photosynthesis: Obligatory role of ubiquinone in photoactive reaction centers of *Rhodopseudomonas sphaeroides*, *Proc. Natl. Acad. Sci. U.S.A. 72*, 3492−3496.

17. Xavier, A. V., and Willson, R. C. (1998) Association and dissociation kinetics of anti-hen egg lysozyme monoclonal antibodies HyHel-5 and HyHel-10, *Biophys. J. 74*, 2036−2045.

18. David, L. (1995) *Handbook of Chemistry and Physics*, 75 ed., CRC, Boca Raton, FL.

19. Lancaster, C. R. (2003) Wolinella succinogenes quinol:fumarate reductase and its comparison to *E. coli* succinate:quinone reductase, *FEBS Lett. 555*, 21−28.

20. Duggleby, R. G., Attwood, P. V., Wallace, J. C., and Keech, D. B. (1982) Avidin is a slow binding inhibitor of pyruvate carboxylase, *Biochemistry 21*, 3364−3370.

21. Xu, Q., and Gunner, M. R. (2002) Exploring the energy profile of the Q(A)⁻ to Q(B) electron-transfer reaction in bacterial photosynthetic reaction centers: pH dependence of the conformational gating step, *Biochemistry 41*, 2694−2701.

22. Kramers, H. A. (1940) Brownian motion in a field of force and the diffusion model of chemical reactions, *Physica 7*, 284−304.

23. Steyaert, J., Wyns, L., and Stanssens, P. (1991) Subsite interactions of ribonuclease T1: Viscosity effects indicate that the rate-limiting step of GpN transesterification depends on the nature of N, *Biochemistry 30*.

24. Kurz, L. C., Weitkamp, E., and Frieden, C. (1987) Adenosine deaminase: Viscosity studies and the mechanism of binding of substrate and of ground- and transition-state analog inhibitors, *Biochemistry 26*, 3027−3032.

25. van Holde, K. E. (2002) A hypothesis concerning diffusion-limited protein−ligand interactions, *Biophys. Chem. 101−102*, 249−254.

26. Schreiber, G. (2002) Kinetic studies of protein−protein interactions, *Curr. Opin. Struct. Biol. 12*, 41−47.

27. Merkler, D. J., Brenowitz, M. S., and Schramm, V. L. (1990) The rate constant describing slow-onset inhibition of yeast AMP deaminase by coformycin analogues is independent of inhibitor structure, *Biochemistry 29*, 8358−8364.

28. Morrison, J. F., and Walsh, C. T. (1988) The behavior and significance of slow-binding enzyme inhibitors, *Adv. Enzymol. Relat. Areas Mol. Biol. 61*, 201−301.

29. Yiallouros, I., Vassiliou, S., Yiotakis, A., Zwilling, R., Stoker, W., and Dive, V. (1998) Phosphinic peptides, the first potent inhibitors of astacin, behave as extremely slow-binding inhibitors, *Biochem. J. 331*, 375−379.

30. Bulow, A., Plesner, I., and Bols, M. (2001) Slow Inhibition of almond glucosidase by azasugars: Determination of activation energies for slow binding, *Biochim. Biophys. Acta 1545*, 207−215.

31. Lohse, A., Hardlei, T., Jensen, A., Plesner, I., and Bols, M. (2000) Investigation of the slow inhibition of almond B-glucosidase and

32. Dharmasena, S. P., Wimalasena, D. S., and Wimalasena, K. (2002) A slow-tight binding inhibitor of dopamine B−monooxygenase: A transition state analogue for the product release step, *Biochemistry 41*, 12414−12420.

33. Jiang, Y. L., Ichikawa, Y., and Striver, J. T. (2002) Inhibition of uracil DNA glycosylase by an oxacarbenium ion mimic, *Biochemistry 41*, 7116−7124.

34. Pandhare, J., Dash, C., Rao, M., and Deshpande, V. (2003) Slow tight binding inhibition of proteinase K by a proteinaceous inhibitor, *J. Biol. Chem. 278*, 48735−48744.

35. Dash, C., Vathipadiekal, V., George, S. P., and Rao, M. (2002) Slow-tight binding inhibition of xylanase by an aspartic protease inhibitor, *J. Biol. Chem. 277*, 17978−17986.

36. Bretscher, E. L., Li, H., Poulos, L. T., and Griffith, W. O. (2003) Structural characterization and kinetics of nitric-oxide synthase inhibition by novel N^5-(iminoalkyl) and N^5-(iminoalkenyl)-orni-thines, *J. Biol. Chem. 278*, 46789−46797.

37. Breton, J., Burie, J., Berthomieu, C., Berger, G., and Nabedryk, E. (1994) The binding sites of quinones in photosynthetic bacterial reaction centers investigated by light-induced FTIR difference spectroscopy: Assignment of the Q_A vibrations in *Rhodobacter sphaeroides* using ¹⁸O- or ¹³C-labeled ubiquinone and vitamin K_1, *J. Am. Chem. Soc. 33*, 4953−4965.

38. Breton, J., Burie, J., Boullais, C., Berger, G., and Nabedryk, E. (1994) Binding sites of quinones in photosynthetic bacterial reaction centers investigated by light-induced FTIR difference spectroscopy: Binding of chainless symmetrical quinones to the Q_A site of *Rhodobacter sphaeroides*, *Biochemistry 33*, 2−24.

39. Steffen, M. A., Lao, K., and Boxer, S. G. (1994) Dielectric asymmetry in the photosynthetic rection center, *Science 264*, 810−816.

40. Warncke, K., and Dutton, P. L. (1993) Experimental resolution of the free energies of aqueous solvation contributions to ligand−protein binding: Quinone-Q_A site interactions in the photosynthetic reaction center protein, *Proc. Natl. Acad. Sci. U.S.A. 90*, 2920−2924.

41. Wells, T., Takahashi, E., and Wraight, C. A. (2003) Primary quinone (Q_A) binding site of bacterial photosynthetic reaction centers: Mutation at residue M265 probed by FTIR spectroscopy, *Biochemistry 42*, 4064−4074.

42. Takahashi, E., Wells, T. A., and Wraight, C. A. (2001) Protein control of the redox potential of the primary quinone acceptor in reaction centers from *Rhodobacter sphaeroides*, *Biochemistry 40*, 1020−1028.

43. Kirmaier, C., Holten, D., and Parson, W. W. (1985) Temperature and detection-wavelenth dependence of the picosecond electron-transfer kinetics measured in *Rhodopseudomonas sphaeroides* reaction centers. Resolution of new spectral and kinetic compontents in the primary charge separation process, *Biochim. Biophys. Acta 810*, 33−48.

44. Okamura, M. Y., and Feher, G. (1992) Proton transfer in reaction centers from photosynthetic bacteria, *Annu. Rev. Biochem. 61*, 861−896.

45. Brzezinski, P., Okamura, M. Y., and Feher, G. (1992) *Structural Changes Following the Formation of D⁺QA⁻ in Bacetrial Reaction Centers: Measurement of Light-Induced Electrogenic Events in RCs Incorporated in a Phospholipid Monolayer*, Plenum Press, New York.

46. Tiede, D. M., and Hanson, D. K. (1992) in *The Photosynthetic Reaction Center II* (Breton, J., and Vermeglio, A., Eds.) pp 341−350, Plenum Press, New York.

47. Zachariae, U., and Lancaster, C. R. (2001) Proton uptake associated with the reduction of the primary quinone Q_A influences the binding site of the secondary quinone Q_B in *Rhodopseudomonas viridis* photosynthetic reaction centers, *Biochim. Biophys. Acta 1505*, 280−290.

48. Xu, Q., and Gunner, M. R. (2000) Temperature dependence of the free energy, enthalpy, and entropy of P⁺QA⁻ charge recombination in photosynthetic reaction centers, *J. Phys. Chem. B 104*, 8035−8043.

49. McPherson, P. H., Okamura, M. Y., and Feher, G. (1988) Light-induced proton uptake by photosynthetic reaction centers from *Rhodobacter sphaeroides* R-26. I. Protonation of the one-electron states D⁺QA⁻, DQA⁻, DAQAQB⁻, and DQAQB⁻, *Biochim. Biophys. Acta 934*, 348−368.

50. Alexov, E. G., and Gunner, M. R. (1999) Calculated protein and proton motions coupled to electron transfer: Electron transfer from

yeast isomaltase by 1-azasugar inhibitors: Evidence for the "direct binding" model, *Biochem. J. 349*, 211−215.

Q_A^- to Q_B in bacterial photosynthetic reaction centers, *Biochemistry 38*, 8253−8270.

51. Nabedryk, E., Bagley, K. A., and Thibodeau, D. L. (1990) A protein conformational change associated with the photoreduction of the primary and secondary quinones in the bacterial reaction center, *FEBS Lett. 266*, 59−62.

52. Miksovska, J., Maroti, P., Tandori, J., Schiffer, M., Hanson, D. K., and Sebban, P. (1996) Distant electrostatic interactions modulate the free energy level of Q_A^- in the photosynthetic reaction center, *Biochemistry 35*, 15411−15417.

53. Kalman, L., Sebban, P., Hanson, D. K., Schiffer, M., and Maroti, P. (1998) Flash-induced changes in buffering capacity of reaction centers from photosynthetic bacteria reveal complex interaction between quinone pockets, *Biochim. Biophys. Acta 1365*, 513−521.

54. Swallow, A. J. (1982) in *Function of Quinones in Energy Conserving Systems* (Trumpower, B. L., Ed.) pp 59−72, Plenum Press, New York.

55. Rich, P. R. (2004) The quinone chemistry of *bc* complexes, *Biochim. Biophys. Acta*, in press.

56. Swallow, A. J. (1982) in *Function of Quinones in Energy Conserving Systems* (Trumpower, B. L., Ed.) pp 59−72, Academic Press, New York.

57. Wraight, C. A. (1998) in *Proceedings of the 11th International Photosynthesis Congress* (Garab, G., Ed.) pp 693−698, Kluwer, Dordrecht, The Netherlands.

58. Dutton, P. L., Leigh, J. S., and Wraight, C. A. (1973) Direct measurement of the midpoint potential of the primary electron acceptor in *Rhodopsuedomonas sphaeroides in situ* and in the isolated state: Some relationships with pH and *o*-phenathroline, *FEBS Lett. 36*, 169−173.

59. Rutherford, A. W., and Evans, M. C. W. (1980) Direct measurement of the redox potential of the primary and secondary quinone electron acceptors in *Rhodopseudomonas sphaeroides* (wild-type) by EPR spectrometry, *FEBS Lett. 110*, 257−261.

60. Prince, R. C., Dutton, P. L., and Bruce, J. M. (1983) Electrochemistry of ubiquinones, *FEBS Lett. 160*, 273−276.

61. Radzicka, A., and Wolfenden, R. (1988) Comparing the polarities of the amino acids: Side chain distribution coeffients between the vapor phase, cyclohexane, 1-octonal, and neutral aqueous solution, *Biochemistry 27*, 1664−1670.

62. Braun, B. S., Benbow, U., Lloyd-Williams, P., Bruce, J. M., and Dutton, P. L. (1986) Determination of partition coeffieients of quinones by high-performance liquid chromatography, *Methods Enzymol. 125*, 119−129.

63. Abraham, D. J., and Leo, A. J. (1987) Extension of the fragment method to calculate amino acid zwitterion and side chain partition coefficients, *Proteins: Struct., Funct., Genet. 2*, 130−152.

64. Hansch, C., Leo, A., and Taft, R. W. (1991) A survey of Hammett substituent constants and resonance and field parameters, *Chem. Rev. 91*, 165−195.

BI050544J